Low-head pumped hydro storage: An evaluation of energy balancing and frequency support

(article starts on next page)

Check for updates

ORIGINAL RESEARCH

Low-head pumped hydro storage: An evaluation of energy balancing and frequency support

Justus Peter Hoffstaedt[1] | **Daan Truijen[2]** | **Antonio Jarquin Laguna[1]** | **Jeroen De Kooning[2]** | **Kurt Stockman[2]** | **Jonathan Fahlbeck[3]** | **Hakan Nilsson[3]**

[1]Faculty of Mechanical Engineering, Department of Maritime and Transport Technology, Delft University of Technology, Delft, the Netherlands

[2]Department of Electromechanical, Systems & Metal Engineering, Ghent University, Kortrijk, Belgium

[3]Department of Mechanics and Maritime Sciences, Division of Fluid Dynamics, Chalmers University of Technology, Gothenburg, Sweden

Correspondence
Justus Peter Hoffstaedt, Faculty of Mechanical Engineering, Department of Maritime and Transport Technology, Delft University of Technology, Mekelweg 2, 2628 CD Delft, the Netherlands.
Email: J.P.Hoffstaedt@tudelft.nl

Funding information
Swedish Research Council, Grant/Award Number: 2022-06725; European Commission - Horizon 2020, Grant/Award Number: 883553

Abstract

Large-scale energy storage solutions are crucial to ensure grid stability and reliability in the ongoing energy transition towards a low-carbon, renewable energy based electricity supply. This article presents the evaluation of a novel low-head pumped hydro storage system designed for coastal environments and shallow seas. The proposed system addresses some of the challenges of low-head pumped hydro storage including the need for larger flow rates and reservoirs as well as the requirement of machinery with high efficiencies across a wide operating range to accommodate larger changes in gross head during storage cycles. It includes several units of contra-rotating reversible pump-turbines connected to axial-flux motor generators within a ring dike, as well as dedicated machine- and grid-side control. The technology allows for independent control of each runner, making it possible to adapt to the specific operating conditions of low-head systems. In this work, a numerical approach is used to simulate the system's performance and dynamic behaviour under various operational conditions, including energy generation, storage, and grid support of a 1 GW system with 4 GWh of storage capacity. The potential system performance for energy balancing cycles is evaluated, and a sensitivity analysis is conducted to assess the influence of scaling the motor-generators on performance and footprint of the plant. Additionally, the capability and limitations of the system to respond to grid demand fluctuations and provide frequency regulation services are assessed. The results demonstrate that the low-head pumped hydro storage system is a viable large-scale energy storage solution, capable of round-trip efficiencies above 70% across a wide operating range. By increasing the maximum power of the electric machines, the maximum head range of the whole system is increased which correlates with a threefold increase in energy density per unit area. The dynamic simulations further show that the system can rapidly change its power output allowing it to provide frequency regulation services. Allocating 20% of its nominal power as a reserve, the new power setpoints can be reached within a maximum of 5 s independent of its initial state of charge.

1 | INTRODUCTION

The integration of renewables into our power grids has gained significant momentum in recent years, driven by the urgent need to mitigate climate change and reduce greenhouse gas emissions. However, rapidly increasing shares of intermittent renewable energy sources, such as wind and solar generators, pose significant challenges to ensure grid stability and reliability [1]. To address these challenges, large-scale energy storage solutions are required to store surplus energy during periods of high production and release it back to the grid during periods of high demand. Energy storage systems should also provide ancillary services, such as frequency regulation and voltage support, further aiding grid stability and reliability [2, 3]. Frequency

regulation plays a crucial role in maintaining the stability and reliability of power systems. Fluctuations in grid frequency, often resulting from a sudden mismatch between electricity generation and demand, can have detrimental effects on the performance of sensitive electrical equipment and even lead to power outages [4]. To address these challenges, energy storage systems can contribute by rapidly injecting or absorbing power in response to frequency deviations, thus helping to maintain grid frequency within a narrow and predefined range.

As of 2020, pumped hydro storage (PHS) provided over 90% of the total global storage capacity [5] and is widely recognised as a suitable solution for grid-scale storage due to its flexible operation, high efficiencies and large storage capacities [6]. It has, however, been limited almost exclusively to high head applications [6, 7] in mountainous regions such as the Swiss Alps in Europe. Since the power and energy capacity of a pumped storage plant is correlated to both the head and the flow rate or storage volume, respectively, lower heads lead to higher flow rates for a given desired power capacity and larger reservoirs for a given energy capacity. Increased flow rates require larger conduits and machinery while larger reservoirs increase the size of the required civil structures. Civil structures alone can contribute up to 60–70% of the total CAPEX of pumped storage plants [8]. These factors have historically meant that low-head applications are economically limited. Low-head compared to traditional high-head pumped storage system also experience larger relative changes in the gross head during a full storage cycle. Consequently, larger changes in flow rates, and with that the operating range of the mechanical equipment (e.g. pumps and turbines), are required to maintain a given power output or input. Therefore, suitable turbo-machinery capable of achieving high efficiencies across a wide operating range in both turbine and pump operation is desired. Additionally, attention should be given to the dynamic response of the system, as larger machinery and mass flow rates can limit the switching time between pump and turbine operation due to the relatively larger inertias when compared to traditional PHS.

Nonetheless, low-head PHS technology has been identified as a significant potential contributor to grid stability [3]. One major factor for the viability of an energy storage technology is its roundtrip efficiency, defined as the ratio between the energy retrieved from storage to the amount of energy initially fed in. Reaching round-trip efficiencies, comparable with traditional PHS systems combined with fast power ramp rates, low-head PHS could reduce the levelised cost of storage but also improve its capability to provide necessary ancillary services, in particular frequency regulation services. With a potential climbing demand for energy balancing and the provision of ancillary services [9], this could allow pumped storage technology to be viable in lowland regions such as the Netherlands, Belgium or Denmark. An initial economic analysis for peak load shifting operation of a potential low-head PHS plant based on German electricity prices has shown that a maximum profit from energy arbitrage of 32.95 M€per 100 MW of installed capacity can be achieved per year [10]. Taking estimates for capital and operational expenditure into account, a grid-scale system would

be profitable with an interest rate of 5% assuming lifetimes of 75–100 years. Considering a 50 year lifespan the system would be profitable for an interest rate below 4.4% [10]. Additional revenue can be achieved by the operator through frequency regulation services. Environmental and legal aspects for low-head pumped hydro storage have been discussed by Ansorena-Ruiz et al. [11] and applicable technologies for low-head systems are reviewed in [7]. The design, performance and behaviour of axial- and mixed flow reversible pump-turbines have been investigated in [12, 13] and [14], respectively.

The goal of this article is to assess the potential performance and dynamic behaviour of a recently developed low-head PHS system with reversible pump turbine (RPT) technology, over its full operating range during energy balancing and the provision of frequency regulation services. This evaluation is based on key indicators such as roundtrip efficiencies, the size of the required reservoir as well as the time to provide 20 % of the systems nominal power as frequency containment reserves (FCR) among others. To achieve this, time-domain simulations of the operation of a grid-scale plant are conducted using both a steady-state and dynamic numerical models. For these simulations, a case study is chosen in which a grid-scale version of the proposed storage plant is applied to a prospective storage site in the Dutch North Sea. Although economic and environmental investigations are not within the scope of this research, the results of this work can provide a good basis and give insight for further analysis of these aspects.

A steady-state model is employed to evaluate the system's performance during a full balancing cycle, which consists of both the complete charging and discharging process. A sensitivity analysis is performed to investigate the effect of scaling the design power rating of the motor-generators on the overall performance and size of the required reservoir for a given desired storage capacity. While the motor-generators are scaled, all other components, notably the RPTs, remain constant. This analysis is motivated by the capability of RPTs to operate beyond their initial design power rating, which is equivalent to the electric machines original rating. To investigate the dynamic behaviour of the plant during the rapid changes of operating points required to provide frequency regulation services, the steady-state model is extended into a dynamic system model. This model covers the most relevant system dynamics and is coupled with a PI-based control algorithm. With this approach, simulations of the plant providing FCR to the electrical grid are performed. Using different initial conditions, these simulations help to understand the potential capabilities and limitations of the system to provide frequency regulation services.

In Section 2, the low-head PHS and RPT technology as well as the prospective storage site selected for the case study are introduced. In Section 3, the steady-state model and characterization of the RPT are elaborated before delving into the extended dynamic modelling approach and the coupled control scheme. In Section 4, the results for the energy balancing and frequency support simulations are presented and discussed. Finally, the conclusions and recommendations for further work are given in Section 5.
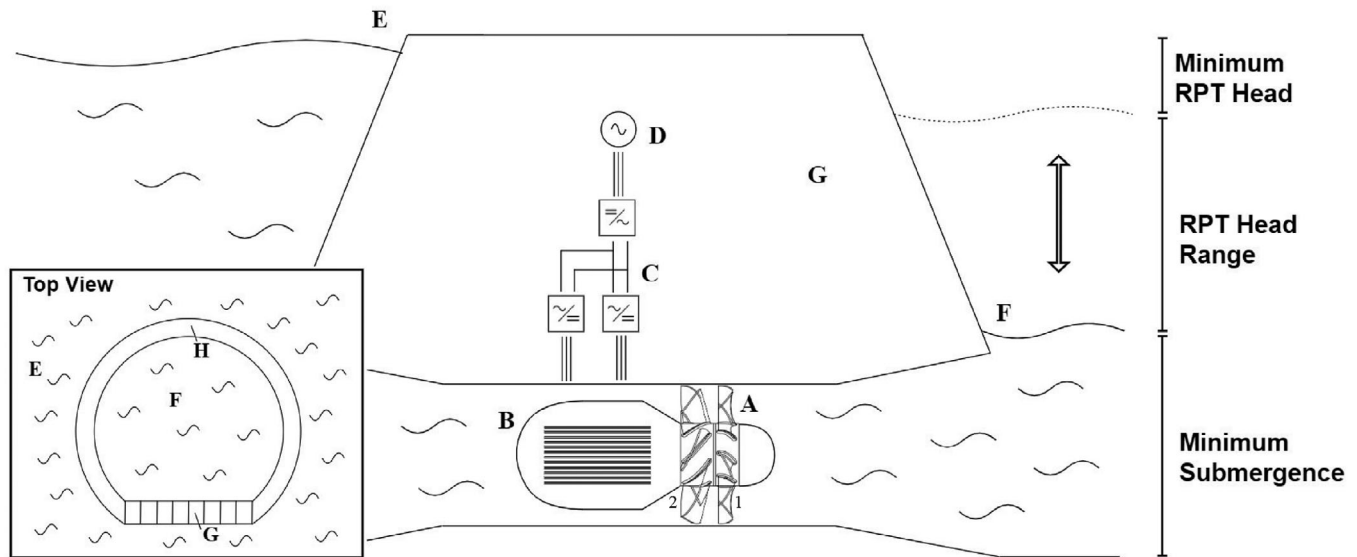
FIGURE 1 Top view and cross-sectional schematic of the proposed low-head pumped storage system showing the contra-rotating runners **A**, axial-flux PMSMs **B**, AC-DC-AC coupling **C**, the electrical grid **D**, the sea as the upper reservoir **E**, the enclosed lower reservoir **F**, the powerhouses **G** and the ring dike **H**.

## 2 | THE LOW-HEAD PHS SYSTEM AND PROSPECTIVE STORAGE SITE

The proposed low-head PHS system is aimed for deployment in shallow seas and coastal environments. It consists of several units of newly developed contra-rotating reversible pump-turbines, axial-flux permanent magnet synchronous machines (PMSM) and a dedicated machine- and grid- side control. This axial-flow approach using two contra-rotating instead of a single runner in combination with axial-flux electric machines has been shown to be a promising solution for low-head applications [7]. This novel approach of using two adjustable speed runners per RPT has distinct advantages for low-head applications. These include increased efficiencies in pump and turbine mode due to a reduction of non-axial flow components as well as a wider operating range at these high efficiencies enabled by the additional control degree of freedom.

A schematic of the system can be found in Figure 1. Similar to conventional pumped storage plants, two reservoirs are needed. In the proposed application in shallow seas, the sea acts as the upper reservoir. A ring dike is deployed encapsulating a basin that serves as the lower reservoir. To store energy, the seawater is pumped out of the inner, lower reservoir to the sea using several sets of RPTs. Conversely, to recoup the stored energy, the reservoir is filled, using the same RPTs in turbine mode. To scale the energy capacity of the plant, the size of the inner reservoir is adjusted. Similarly, to scale the power capacity of the plant the number of RPT sets is varied. Each set of RPT and coupled axial-flux electric machines has an initial design power rating of 10 MW. The RPT has a diameter of 6 m and is designed for a head range of 2–20 m [3, 13].

The site for the case study is located in the Dutch North Sea as shown in Figure 2, selected due to the Dutch Government's commitment to developing several large-scale wind farms within the Dutch Exclusive Economic Zone [15, 16].

This region is characterised by its favourable wind conditions and relatively shallow waters, which not only make it ideal for offshore wind farm installations but also the addition of a large-scale low-head pumped hydro storage system. By creating an energy hub in that location with storage capabilities adjacent to renewable generators, several benefits can be achieved. First, short distances between the storage plant and generators can significantly reduce the transmission losses and cost of infrastructure [17]. Second, additional interconnectors can be created to neighbouring countries bordering the North Sea region, further promoting the integration of renewable energy into the wider European grid. Lastly, by sharing parts of the civil structures with offshore wind farms, some of the high upfront cost can be shared.

Aside from the proximity to energy infrastructure, one of the main factors to consider for the site assessment is the local bathymetry, since the sea depth defines the available gross head. The proposed site has a sea depth of approximately 28 m and is assumed constant for the whole area of the reservoir. Based on the runner diameter of 6 m, an inlet/outlet diameter of 10 m and a minimum submergence depth of 2 m, the available head range is 2–16 m, assuming no submergence of the RPT units under the seabed. While the RPT itself is hydraulically designed for heads of up to 20 m, the 10 MW power rating of the motor-generators severely limits the usable head range, particularly the maximum head in pump mode. The tidal range for the proposed site is around 1.5 m [18]. For this study, the tidal influence on the gross head is neglected since the impact of a tidal cycle with a minor tidal range should average out with time when asynchronous to the storage cycle of the plant. With each set of the proposed RPT being rated at 10 MW, the whole system is initially scaled to a design power capacity of 1 GW utilising 100 RPT units with a total net storage capacity of 4 GWh. Other factors for the site assessment include the composition of the local seabed since a large clay layer is required to seal the
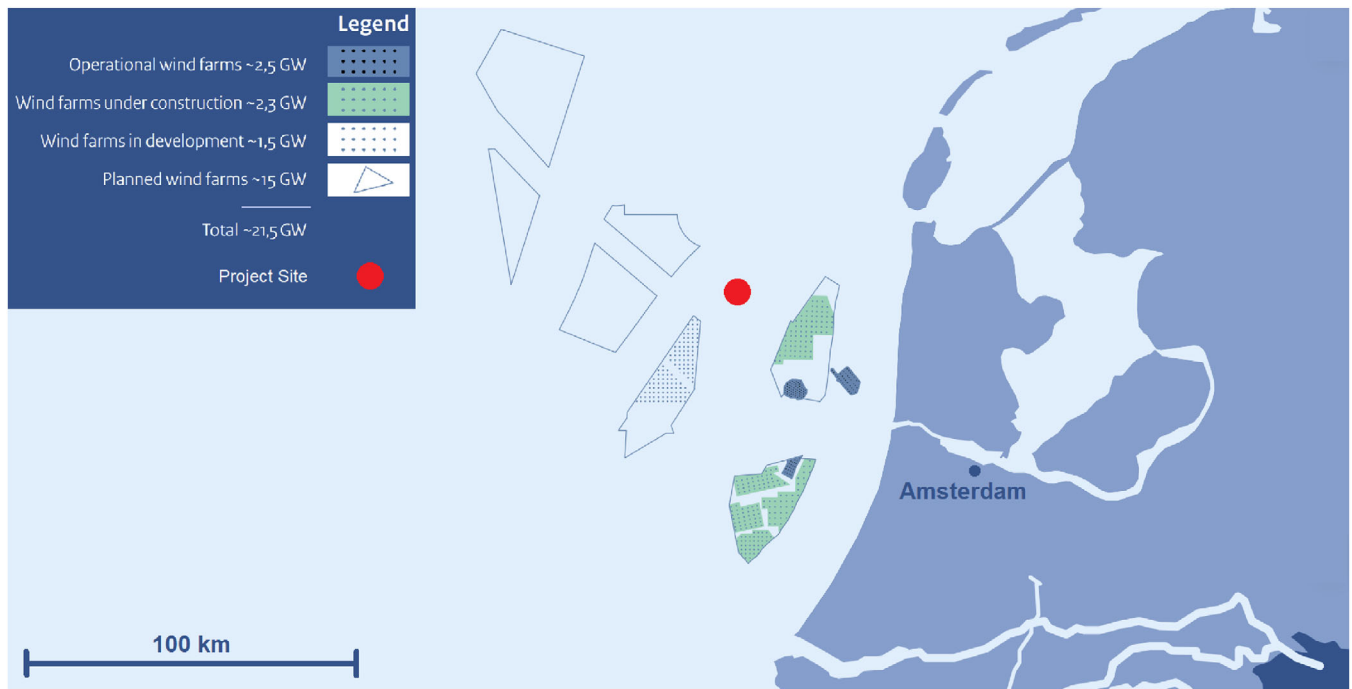
FIGURE 2 Location of the site for the proposed low-head pumped storage plant in the Dutch North Sea (adapted from [16]).

bottom of the reservoir and avoid excessive seepage. Wave conditions that may restrict the construction process and type of dams used must also be considered, along with other legal and environmental aspects for which further information are given in [11].

3 | NUMERICAL MODEL AND PUMP-TURBINE CHARACTERISATION

To assess the low-head pumped storage system introduced in the preceding chapter, two separate numerical models are employed. For the long-term energy balancing simulations, a steady-state model is used. Since the main goal of these simulations is to assess the overall performance in pump and turbine modes, a quasi static approach allowed for the simulation of larger timescales without including any transient operation. When investigating the system's capability to rapidly change operating points and provide frequency regulation services, the entire plant's dynamic response needs to be accounted for and included in the simulations. Thus, a dynamic system model covering the conduits hydraulic transport, the RPT and the drivetrains coupled to a PI-based control algorithm is implemented.

3.1 | Pump-turbine characterisation

For both of these modelling approaches, one core aspect is the characterisation of the newly developed RPT. The two contra-rotating runners that the RPT consists of are shown
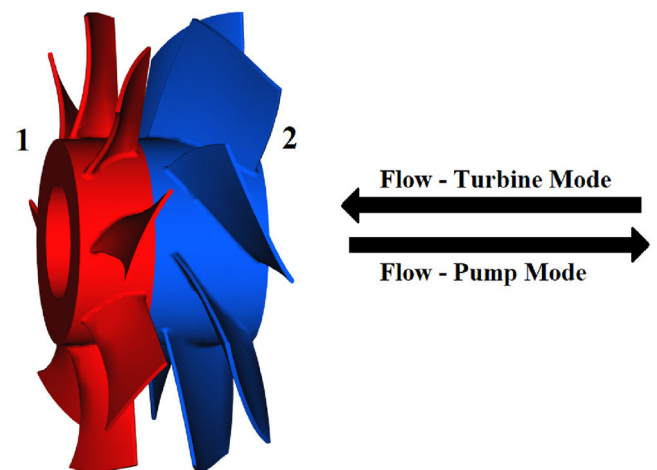
FIGURE 3 Low-Head RPT consisting of two contra-rotating runners with a diameter of 6 m, a design power rating of 10 MW and design flow rate of 130 m^3/s. Runner 1 is shown in red and runner 2 in blue.

in Figure 3. Runner 1, shown in red, is the downstream runner in turbine mode. Conversely, runner 2, indicated in blue, is the downstream runner in pump mode. In both turbine and pump modes, runner 1 rotates clockwise, while runner 2 rotates counter-clockwise relative to their respective flow directions.

The characterisation is based on 180 steady-state computational fluid dynamics (CFD) simulations as per Fahlbeck et al. [19] covering the operating range in both pump and turbine mode. The simulation's computational domain included one blade passage per runner with an infinitely long hub. Since the system can vary the rotational speeds of both runners,

resulting in adjustable speed ratios between them, the runners were characterised individually using their tip speed ratios. These are defined as the ratio between the tangential speeds of the tips of the runners, calculated from the rotational speeds $\omega_{1,2}$ and runner radius R and the average flow velocity u as per:

$$\lambda_{1,2} = \frac{\omega_{1,2} R}{u}. \tag{1}$$

The tip speed ratio can also be interpreted as the inverse of the dimensionless flow coefficient which is commonly used in turbo-machinery literature. Using a non-linear polynomial regression, the CFD results covering most of the operating range of the RPT in pump and turbine modes, are translated into dimensionless head coefficients $C_{h1,2}$ and efficiencies $\eta_{1,2}$ as a function of both runners' tip speed ratios $\lambda_{1,2}$. The head coefficients are defined as the pressure difference across each runner, with the runner heads $H_{r1,2}$, the fluid density ρ and the gravitational acceleration g, divided by the dynamic pressure:

$$C_{h1,2} = \frac{\rho g H_{r1,2}}{\frac{1}{2}\rho u^2}. \tag{2}$$

The efficiencies of the runners are defined, in turbine mode, as the mechanical power of the runners given by the rotational speeds and hydraulic torques $\tau_{h1,2}$ divided by the available hydraulic power to each runner with the runner heads, the volumetric flow rate Q, the fluid density and the gravitational acceleration:

$$\eta_{1,2} = \frac{\omega_{1,2}\tau_{h1,2}}{\rho g Q H_{r1,2}}. \tag{3}$$

For pump mode, the efficiency is defined as the inverse of Equation (3). Finally, the average flow velocity is calculated using the volumetric flow rate and the entire cross-sectional area of the conduit at the runners location.

The characterisation of runner 1 and 2 are given for turbine mode in Figure 4. Figures 4a and 4c show the head coefficients of runner 1 and 2, respectively, as a function of the tip speed ratio of runner 1. The different curves in the graph represent different proportions between the runners' tip speed ratios. Figures 4b and 4d show the corresponding efficiencies of the runners. As evident from all graphs, the speed ratios between the two runners affect the performance of each one individually. Runner 1 sees a fairly consistent increase in head coefficient as the tip speed ratios decrease. However, its efficiency clearly shows a range of peak performance that is shifting slightly as the ratio between the runners is adjusted. In the range of tip speed ratios between 2.5 and 3.25, efficiencies above 0.9 and peaking around 0.95 are achieved. Runner 2 has a much wider operating range with more constant head coefficients and high efficiencies with an overall maximum of around 0.97 and a maximum of 0.9 within the operating range that is ideal for runner 1. A similar characterisation of both runners was obtained in pump mode.

3.2 | Steady-state model

The steady-state model is used to run long-term simulations of the full charge and discharge process. This model is based on the RPT characterisation, modelling of the other hydraulic components such as the valve and reservoir, approximations of the hydraulic and drivetrain losses and the control. The control dictates a power setpoint for any given RPT head, as the reservoir empties and fills. This is required since the storage system experiences a wide relative range of gross heads and for each of these heads different operating points can be reached by adjusting three control degrees of freedom. These are the rotational speeds of both RPT runners as well as the opening angle of a flow control valve used at the high pressure side of the RPT. To obtain the combination of these parameters that reach the highest efficiency for all possible power setpoints at any given head, the steady-state RPT characterisation is used in combination with approximations of the hydraulic and drivetrain losses of the system. The resulting rotational speeds and valve opening angles to reach these operating points as well as the resulting flow rate are stored in lookup tables. The choice of power setpoint for any given head during the storage cycle is based on the setpoint offering the highest efficiency. In turbine mode, this correlates with the maximum power available. Conversely, in pump mode, the highest efficiency points lie between the minimum and maximum power. However, if the efficiency difference for two sets of points is under one percent, roughly the error margin of the characterisation, the point with the higher power is preferred. A comprehensive examination of the pump-turbine curves, the potential control strategies and all lookup tables used in these simulations are given by Truijen et al. [20]. During the simulations, the model obtains the net RPT head based on the gross head between the reservoirs, the hydraulic losses and the valve. Together with the desired power setpoints, the operating conditions are obtained for each point from the lookup tables.

The major hydraulic losses, H_{lmaj}, are approximated using the Darcy-Weisbach equation [21],

$$H_{lmaj} = f\frac{L}{D}\frac{u^2}{2g}, \tag{4}$$

with L as the conduit length and D as the conduit diameter. The Darcy friction factor f, is obtained from a version of the Colebrook-White equation for fully turbulent flow with ε as the pipe roughness height [22]:

$$f = \left(\frac{1}{-2\log_{10}\left(\frac{\varepsilon}{3.7D}\right)}\right)^2. \tag{5}$$

In the expected operating range of the storage system, the Reynolds number is above 7×10^6, therefore in highly turbulent flow conditions, the influence of viscosity in the head losses becomes negligible, and the flow is primarily affected
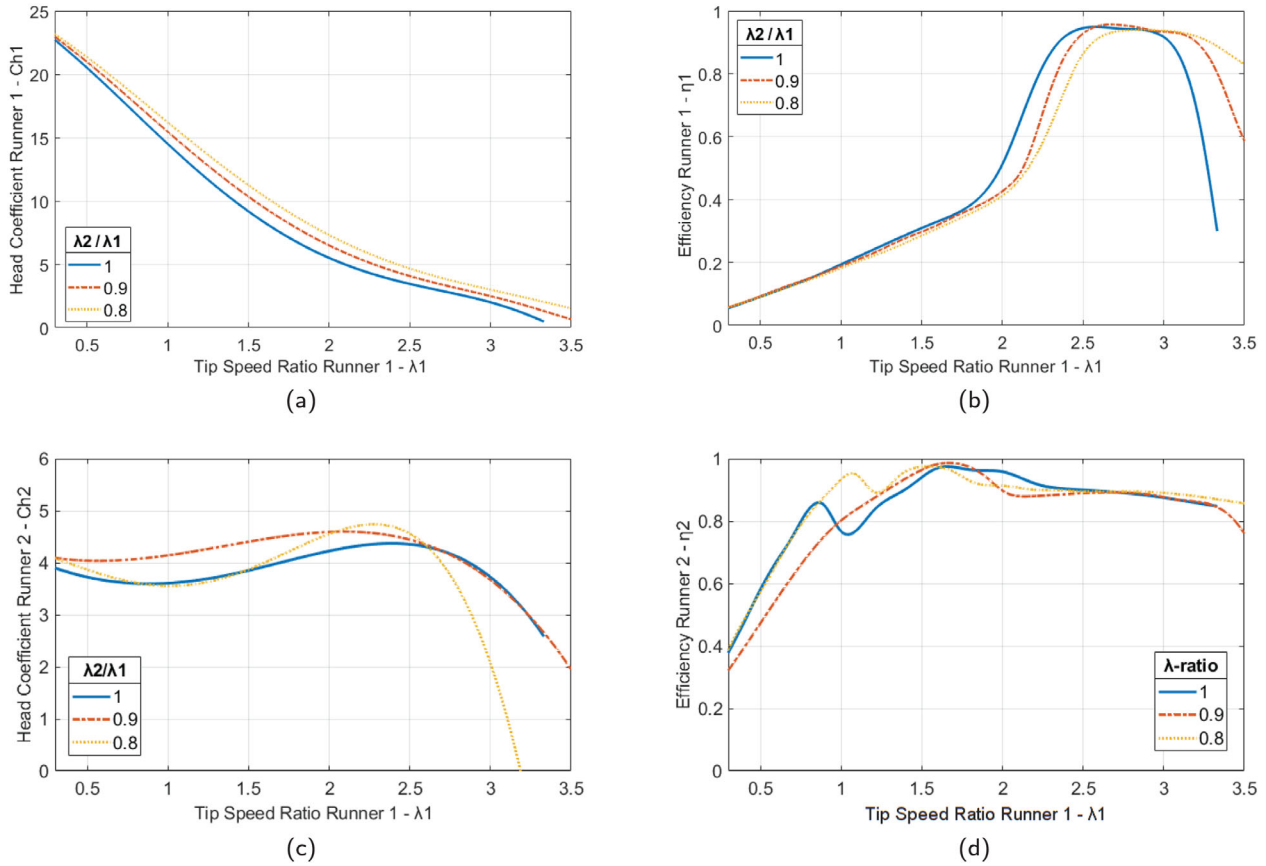
FIGURE 4 Characterisation of runners 1 and 2 in turbine mode as a function of the tip speed ratio of runner 1 for different operational tip speed ratios of runner 2. (a) Head coefficient runner 1. (b) Efficiency runner 1. (c) Head coefficient runner 2. (d) Efficiency runner 2.

by the roughness of the pipe. The minor losses, H_{lmin}, caused by hydraulic and conduit components such as bends, vales and expansions/contractions are approximated in a similar manner, using k as the minor loss coefficient [23]:

$$H_{\text{lmin}} = k \frac{u^2}{2g}. \tag{6}$$

The valve head loss is calculated based on a minor loss coefficient k_{v}, defined as a function of its normalised opening angle γ, with values between $0 \le \gamma < 1$ as per,

$$k_{\text{v}} = \frac{\frac{1348}{75}\gamma^3 - \frac{41}{5}\gamma^2 + \frac{128}{75}\gamma}{(1 - \gamma)}, \tag{7}$$

and shown in Figure 5, obtained from the loss coefficient values given for a gate valve in [24]. Here, a value of zero corresponds to a fully open valve. Although the model excludes any unsteady effects in the RPT behaviour and transient operation of the storage plant, it does account for slow changes in the reservoir water level based on the conservation of mass. The changing height in the reservoir water level H_{res} is therefore given by in- or outgoing flow rate and the reservoir area A_{res}, which is assumed uniform along the reservoir's height:

$$\frac{\mathrm{d}H_{\text{res}}}{\mathrm{d}t} = \frac{Q}{A_{\text{res}}}. \tag{8}$$
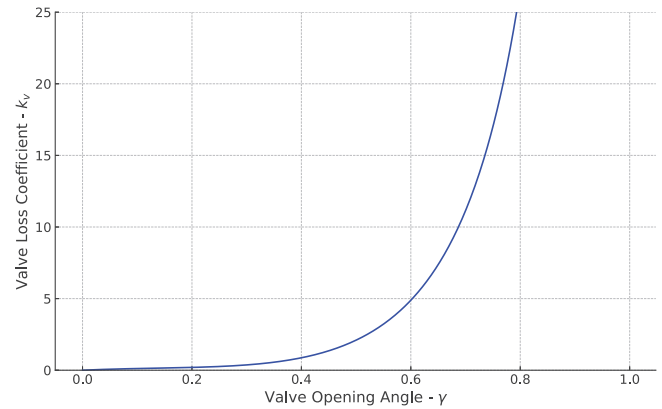
FIGURE 5 Valve loss coefficient k_y as a function of its opening angle γ.

3.3 | Integrated dynamic model

In order to evaluate the potential and limitations of the system to provide frequency regulation services, the steady-state model is extended to include dynamic effects of the most pertinent system components, notably the conduit, both drivetrains, the flow control valve and the control system. The resulting coupled algebraic and ordinary differential equations (ODE) that represent the behaviour of the main components, are implemented and solved through numerical ODE integration schemes. A schematic overview of these components and how they are
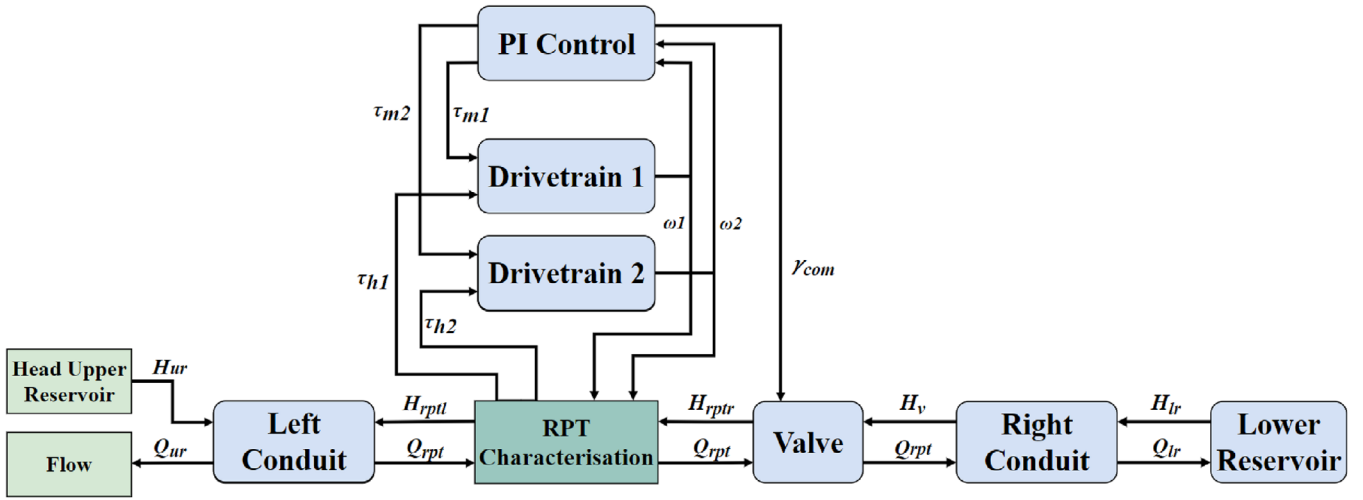
FIGURE 6 Schematic overview of the system model showing the numerical interactions and coupling between components. In blue are model components with dynamic effects, in dark green steady-state components, and in light green the inputs/outputs.

numerically coupled is given in Figure 6. The discrete conduit model, assessing the temporal and spatial changes of flow rates and pressure heads, is divided into two sections: the high-pressure section on one side of the RPT and the low-pressure section on the other. The high-pressure conduit takes the static head of the upper reservoir, denoted as H_{ur}, and the high-pressure RPT head H_{rptl} as inputs. This produces the flow rate to the upper reservoir Q_{ur} and the RPT flow rate Q_{rpt}. Notably, the RPT flow rate remains constant until it is fed into the low-pressure conduit. Contrary to the high-pressure conduit, it uses one flow rate and one pressure head, the one of the lower reservoir H_{lr}, as inputs. The outputs are the flow rate into the lower reservoir Q_{lr} and the head of the valve H_v. Depending on the flow rate and valve opening angle, driven by the opening angle command γ_{com}, the valve provides the low-pressure RPT head H_{rptr} to the RPT characterisation. The tip speed ratios of both runners are calculated from the flow rate and both rotational speeds, which are obtained from the individual drivetrain models. With these, the head coefficients and efficiencies of both runners are obtained. Finally, the hydraulic torques of both runners and the machine torques $\tau_{m1,2}$ set by the control algorithm are given to the drivetrain models. Following, the numerical approach for each component is given. This methodology follows a similar implementation and solution as presented in [25].

3.3.1 | Conduit, valve and reservoir

Low-head PHS systems are characterised by larger mass flow rates of water for a given desired power capacity when compared to high head applications. To cover potential transient behaviour, commonly known as water hammer effects, that could be caused by the increased water conduit inertia and sudden changes in the operating conditions, a numerical approach considering the compressibility of water is chosen to account for the dynamic effects. The used equations are based on

the conservation of mass and momentum, respectively, for a horizontal rigid pipeline with constant cross-section [26–28]:

$$\frac{\partial H}{\partial t} = -\frac{a^2}{gA}\frac{\partial Q}{\partial x}, \tag{9}$$

$$\frac{\partial Q}{\partial t} = -gA\frac{\partial H}{\partial x} - \frac{fQ|Q|}{2DA} - \frac{k_u}{g}\left[\frac{\partial Q}{\partial t} + \text{Sign}(Q)a\left|\frac{\partial Q}{\partial x}\right|\right]. \tag{10}$$

With these one-dimensional coupled partial differential equations, the change in pressure head and flow acceleration can be obtained with H as the pressure head, a the pressure wave velocity, A the conduit cross-sectional area, and k_u as the unsteady loss coefficient. Steady losses are considered using the Darcy-Weisbach equation and unsteady losses using an instantaneous acceleration-based method [29], both included in Equation (10). The Darcy friction factor is assumed constant and the effect of the Reynolds number neglected due to the highly turbulent flow as discussed in Section 3.2. The pressure wave velocity is also assumed constant. Additional minor losses such as entrance and exit losses are included at the boundaries using the minor loss equation as shown in Equation (6). For the numerical approach, the partial derivatives with respect to space, are replaced by algebraic equations using a second order central-schemed finite difference method. The consequential spatial discretisation combined with the chosen timestep results in a grid of nodes, for each of which the pressure and flow are calculated. Dirichlet boundary conditions are imposed accordingly for the upstream and downstream pressures and flow rates. Finally, the valve actuator response is modelled with a first order linear approach for the opening angle with the dynamic response driven by the time constant T_v and the opening angle command:

$$\frac{d\gamma}{dt} = \frac{1}{T_v}(\gamma_{com} - \gamma). \tag{11}$$
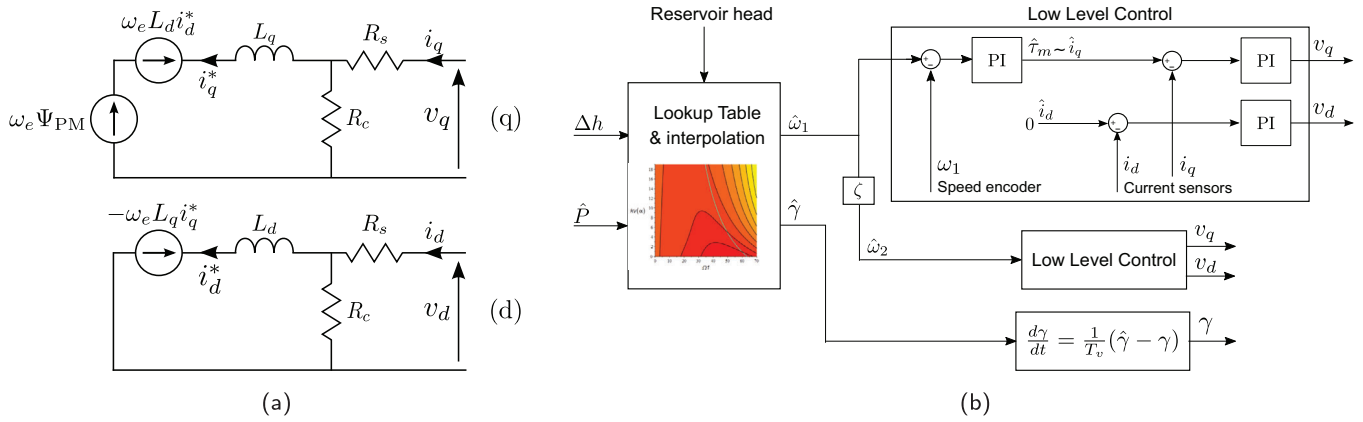
FIGURE 7 (a) Equivalent scheme of an axial-flux PMSM in the rotating *dq* reference frame. (b) Schematic overview of the applied control architecture.

3.3.2 | Drivetrain and RPT

The proposed system employs a variable speed direct drive without any gearing between the two runners and their respective axial-flux PMSM. The main components of the drivetrains are the runners, driveshafts and rotating parts of the electric machines. The rotational speed of the drivetrains are modelled using the equation of rotational motion:

$$J_{1,2}\frac{d\omega_{1,2}}{dt} + D_{f1,2}\omega_{1,2} = \tau_{h1,2}(\lambda_1, \lambda_2) - \tau_{m1,2} \quad (12)$$

Consequently, the rotational speeds are calculated based on the balance between hydraulic and machines torques. In this rigid body approach, any torsional flexibility is neglected resulting in one lumped rotational mass moment of inertia J per drivetrain. Additionally, the drivetrain friction losses are represented by a viscous damping torque coefficient $D_{f1,2}$ determined as a percentage of the nominal torques at the nominal rotational speeds.

With the flow rate as well as the efficiencies and heads of the runners, obtained from the RPT characterisation as a function of both tip speed ratios, the hydraulic torques are obtained from the total power and the rotational speeds:

$$\tau_{h1,2}(\lambda_1, \lambda_2) = \frac{\rho g Q H_{r1,2}(\lambda_1, \lambda_2)\eta_{1,2}(\lambda_1, \lambda_2)}{\omega_{1,2}}. \quad (13)$$

The machine torques are altered by the control architecture as outlined in the following section.

3.3.3 | Axial-flux PMSMs and control architecture

The axial flux PMSMs are modelled in the rotating *dq* reference frame (Figure 7a), where the stator inductances, the armature reaction, the stator losses and the iron losses (comprising eddy current and hysteresis losses) are included [30]. Figure 7b visualises the applied control architecture. Here, the circumflex '^' indicates a setpoint for a certain variable. From the lookup table

discussed in Section 3.2, the rotational speed setpoints $\hat{\omega}_{1,2}$ and valve angle $\hat{\gamma}$ can be found that reach the power setpoint at the current head with the highest efficiency. For each machine, the speed setpoint is fed to a cascaded speed controller. Based on the difference between the speed setpoint $\hat{\omega}$ and the measured speed ω, a first PI controller defines the torque setpoint τ_m. Next, this machine torque is controlled using field oriented control. Here, the i_d current is regulated to zero, resulting in a directly proportional relation between the i_q current and the machine torque. Therefore, a torque setpoint $\hat{\tau}_m$ from the speed PI-controller directly translates to a current setpoint $\hat{i}_q$. Based on the difference between the $\hat{i}_{d,q}$ current setpoints and the measured current $i_{d,q}$, PI controllers define the applied voltages $v_{d,q}$.

These cascaded PI controllers are tuned by optimally shaping the step response in terms of rise time, settling time and overshoot of the torque and speed setpoints. Additionally, in order to ensure stability and robustness, the parameters are tuned to have a gain and phase margin of, respectively, >10 dB and $> 45°$ over the operating range. Although this guarantees a fast power response, it can cause fluctuations during the power response rise time. This is due to how the speed PI-controller uses the torque as a means to control the speed. If a new power setpoint (and thus new speed setpoints) is applied, the PI-controller outputs a torque that scales with the error between the new speed setpoint and the current speed. As this error is high initially, the output torque setpoint is either very low or very high. As the power is a product of speed and torque, this means that the higher the torque actuation, the higher the power fluctuation during transition periods. As an example, if a power setpoint is increased in turbine mode and this corresponds to an increase in rotational speeds, the machine torques will decrease to allow the hydraulic torque to speed up the RPT, resulting in an initial power decrease before increasing to the higher power setpoint once the rotational speeds are reached. Therefore, a dynamic torque constraint is designed to limit the fluctuation of the power response to a predefined value P_{fl}. On a power setpoint $\hat{P}$ change on time t_0, the measured individual powers at this time $P_{1,2}(t_0)$ are saved. Next, the stored data in the lookup tables is addressed to find the individual powers $\hat{P}_{1,2}$ for the new power
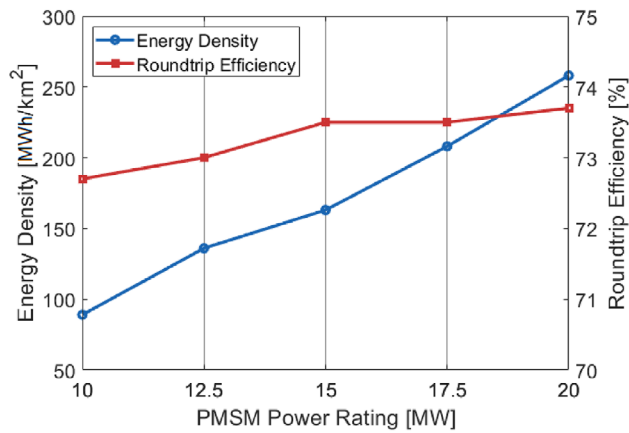
FIGURE 8 Energy density and round-trip efficiency of the pumped storage system as a function of the power rating of the electric machines.

setpoint. Then the machine torque setpoints are constrained until the power setpoint is reached according to:

$$\frac{\min\left(P_{1,2}(t_0), \hat{P}_{1,2}\right) - P_{fl}}{\omega_{1,2}(t)} < \tau_{m1,2}(t) < \frac{\max\left(P_{1,2}(t_0), \hat{P}_{1,2}\right) + P_{fl}}{\omega_{1,2}(t)}. \tag{14}$$

4 | SIMULATION RESULTS

4.1 | Energy balancing

At the selected storage site, the available gross head range is 2–16 m. Using the proposed PMSMs with a power rating of 10 MW each, the maximum achievable head is 9 m; however, since the power rating of the electric machines is otherwise exceeded in pump mode. The RPTs have a much wider operating range though and can therefore be operated at higher hydraulic powers. Using the steady-state model, simulations of the full balancing cycle, including pump and turbine modes, have been carried out. Iteratively, the power rating of the electric machines is increased between 10 and 20 MW in 2.5 MW steps. The objective of these simulations is to evaluate the performance and operational conditions of the plant throughout the full cycle as well as the required reservoir size and cycle times. The major outputs are therefore the efficiencies of both runners, the total power output, the flow rate, the net head of the RPT unit and the water level in the lower reservoir. All simulation parameters related to major and minor hydraulic losses as well as the drivetrain losses are identical to the dynamic simulations and can be found in Table 2.

Increasing the power rating of the PMSMs correlates almost linearly with an increase in the maximum achievable gross head. Increasing the head range consequently results in a steep rise in storage capacity per unit area. This change in energy density as a function of PMSM power rating as well as the corresponding change in round-trip efficiency over the full cycle are shown in Figure 8. An overview of the results from the cycle simulations are also given in Table 1.

TABLE 1 Comparison of simulations for varying PMSM power ratings.

PMSM power rating	10	12.5	15	17.5	20	MW
Max. head	9	11	12	13.5	15	m
Reservoir area	44.8	29.4	24.5	19.2	15.5	km^2
Average power (per RPT unit)	5.2	6.6	7.3	8.5	9.6	MW
Time pump mode	9:33	7:33	6:39	5:46	5:07	hh:mm
Time turbine mode	8:44	6:54	6:14	5:24	4:45	hh:mm

By doubling the power rating of the PMSMs the energy density increases almost threefold while the round-trip efficiency changes very little and even increases by about 1%. For the proposed plant with a desired net energy capacity of 4 GWh this means a reduction in reservoir area from 45.5 km^2 to 15.6 km^2. The average power per RPT unit also increases from 5.2 MW to 9.6 MW (0.52 GW and 0.96 GW for the full plant) reducing the time for a full cycle from 18 h and 17 min to 9 h and 52 min. Comparing the balancing cycle of the 10 and 20 MW PMSMs, the water level in the lower reservoir and the flow rate per RPT unit over the full cycle are shown in Figure 9. For both cases, the storage system is initially fully discharged leading to different initial water levels in the reservoir. It should also be noted that a reservoir level of zero does not correspond to a fully emptied reservoir but rather the minimum possible water level in the reservoir determined by the minimum submergence of the RPT inlets as illustrated in Figure 1. The reservoir levels decrease as the RPTs operate in pump mode emptying the reservoir and thereby charging the storage system. Once the reservoir reaches its minimum, the plant switches to turbine mode, indicated by the red vertical line in the graphs. As the flow rates invert, the reservoir is filled again and the storage system discharged.

The minimum flow rates are the same with both power ratings of the electric machines with around 57 m^3/s in pump mode and 60 m^3/s in turbine mode. The maximum flow rate is increased using the 20 MW version of the PMSMs to around 161 m^3/s from 135 m^3/s in turbine mode and to 141 m^3/s from 123 m^3/s in pump mode. Generally, the change in flow rate is a direct result of the changing power setpoint and head of the RPT with the last remaining influencing factor being the slightly fluctuating RPT efficiency. This can be specifically observed towards the end of the pump cycle with the 10 MW PMSMs as the flow rate increases with the increasing power setpoint. Once the maximum power of 10 MW is reached, the increasing net head of the RPT causes an almost linear decrease in flow rate.

The charging and discharging power per RPT unit as well as the efficiency of the plant during the full cycle are shown in Figure 10. The efficiency includes all hydraulic as well as drivetrain losses but excludes losses in the electric machines and converters. Over the full cycle in both pump and turbine mode, high efficiencies mostly in the range of 82–87% are achieved. The minimum efficiency appears in pump mode at the beginning of the cycle where the gross head is the smallest. No clear correlation is visible between the overall efficiency and the
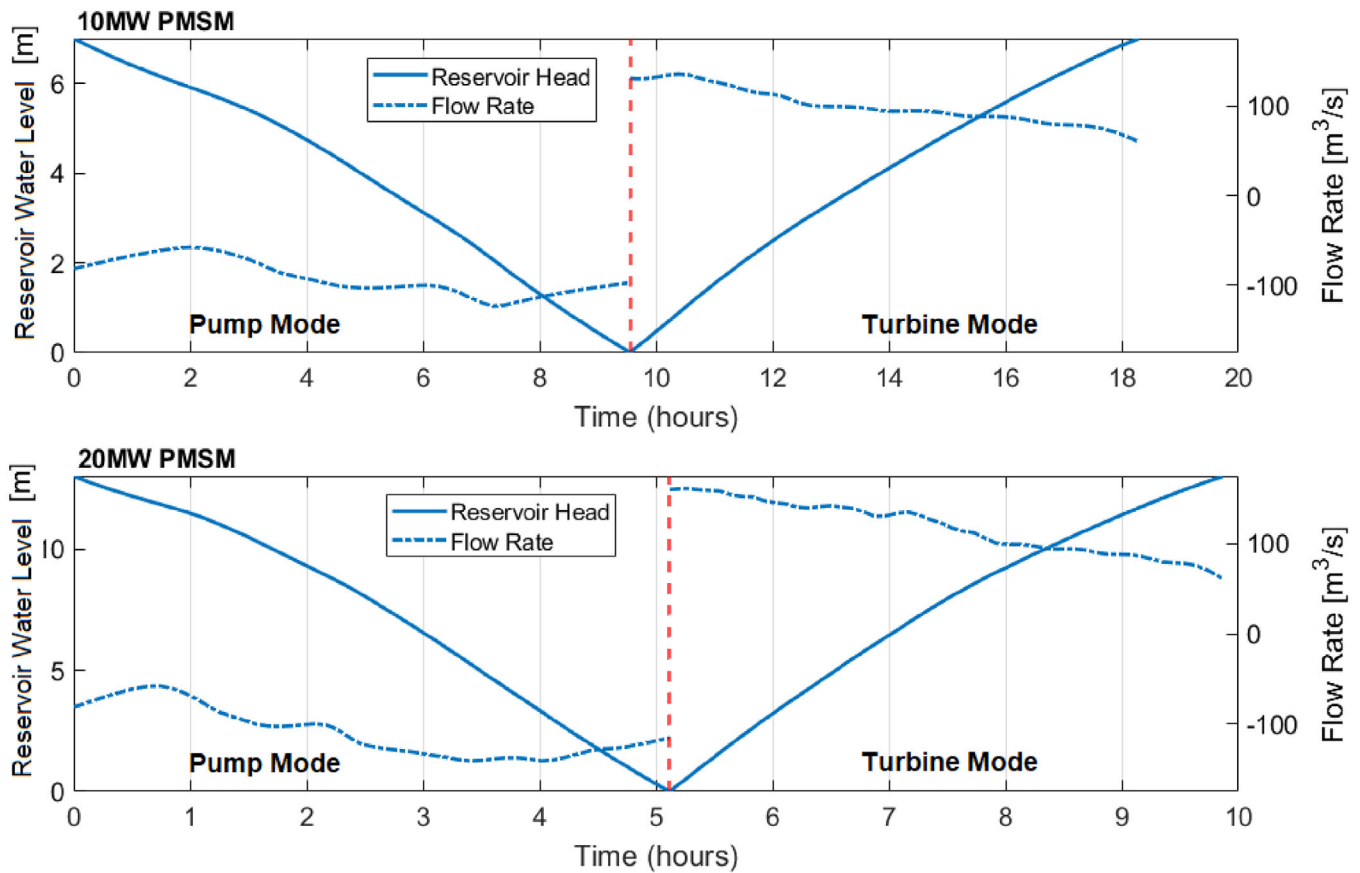
FIGURE 9   Reservoir head of the storage plant and flow rate of each RPT unit over a full balancing cycle compared for a 10 and 20 MW PMSM.

hydraulic losses suggesting that the efficiency is mostly determined by the RPT characteristics as the operating points change. Some of the minor fluctuations in the efficiency deviating by less than 1% are also caused by the resolution of the lookup tables and the required interpolation between the datapoints. The maximum power capacity for both cases and both modes is only reached during a small part of the cycle as the maximum head is approached.

With no overall loss in performance and a maximum increase in flow rate of 19%, the apparent major disadvantage of using the scaled up version of electric machines is the requirement of an additional PMSM per RPT unit. Since the electric machines are located in the bulb adjacent to the runners, increasing the power capacity of the existing machines is constrained since that would result in an increase in diameter. This would, in turn, enlarge the bulb causing higher hydraulic losses. Instead, a second PMSM unit can be attached to the same drivetrain doubling the torque and power capacity. The additional cost and complexity of adding a second electric machine to each RPT should be offset by the significantly reduced reservoir size that is required for the desired 4 GWh energy storage capacity. The dam would be shortened from a total length of 95 to 56 km. Although it is worth noting that for alternative storage sites with a shallower sea depth, the larger reservoir size required when limiting the power rating of the electric machines to 10 MW

could be partially offset by a reduction in dam height of 6 m. In addition to the economic benefits, a reduced reservoir size also alleviates environmental and legal concerns. Furthermore, the increase in average power input and output and the corresponding reduction in cycle time should further help to improve the economics.

For energy balancing, the evaluated plant demonstrates comparable performance at grid-scale to conventional high-head pumped storage plants, which are typically sized between 1 and 1.5 GW and achieve roundtrip efficiencies ranging from 70% to 80% [6]. The major disadvantage of the plant is its reduced energy density. However, in regions without suitable topography for high-head applications, alternative concepts can unlock the use of pumped storage technology. Other such amended concepts include subsea energy storage, gravity energy storage and underground pumped storage. These have theoretical roundtrip efficiencies of up to 73%, 80% and 77%, respectively [31–33]. While promising, these technologies also face challenges and limitations regarding the required civil structures, suitable sites and scale that can be reached. At grid scale and balancing at similar timescales as LH-PHS, compressed air energy storage and battery energy storage are commonly discussed. Compressed air energy storage currently achieves roundtrip efficiencies of 42–55% and lithium-ion batteries reach over 90% [34]. Due to the high performance and scalability of lithium-ion batteries
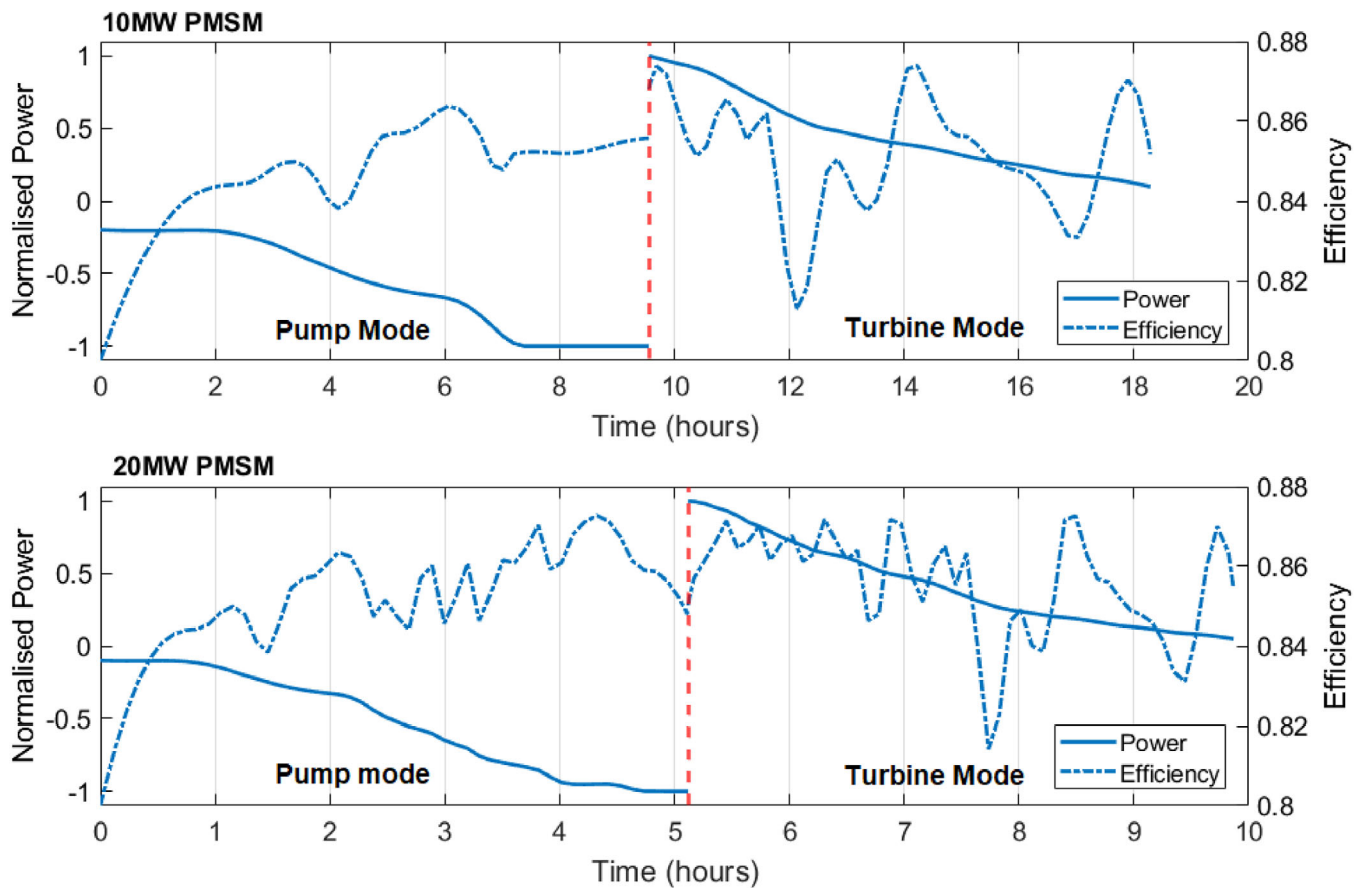
FIGURE 10   Power and efficiency of the storage plant over a full balancing cycle compared for a 10 and 20 MW PMSM.

they have seen significant uptake in recent years but also face safety as well as environmental concerns regarding recycling, extraction and toxicity of the raw materials needed [35, 36].

To suit different applications, a heterogeneous pool of storage technologies is needed. While further economic and environmental assessments are required, the results presented demonstrate the technical potential of LH-PHS to contribute to that pool with grid-scale energy balancing.

4.2 | Potential to provide frequency regulation services

While PHS systems are widely recognised for their potential in short and long-term energy balancing, this section focuses on the capability of the proposed system to provide frequency regulation services. This system, similar to most renewable generators, is coupled to the grid via inverters and therefore does not provide inherent grid coupled inertia. It can, however, directly contribute to grid stability through frequency regulation by rapidly absorbing or injecting power into the grid. The main limitation to provide these services is how quickly the system can vary its power output, which in the case of PHS is largely determined by its mechanical and hydraulic characteristics. Key factors include the inertia of the drivetrain, power-takeoff, and

the hydrodynamics of the conduit. Sudden changes in flow rate may also induce transient pressure waves commonly known as water hammer effects, a significant concern for system stability and safety. The plant's control system design and tuning also have a considerable effect on the responsiveness of the plant.

The dynamic system model presented in Section 3.3 is implemented in the commercial platform MATLAB-Simulink using a fixed step solver with a sample time of 1 ms. All simulations start in steady-state from a defined operating point and have a simulation time of 13 s. For the spatial discretisation, 40 nodes are used. Standard values from the literature are used for unknown loss coefficients, surface roughness etc. Table 2 gives an overview of all used parameters. The model includes all hydraulic and drivetrain losses, and contrary to the steady-state model also the losses in the electric machines and AC-DC-AC coupling. Excluded from the analysis are the potential hydraulic losses from the bulb used adjacent to the runners containing the PMSMs.

To evaluate the system's potential to provide frequency regulation services, simulations of providing frequency containment reserve are carried out; 20% of the nominal power of the plant is reserved for this. Such an FCR response would be triggered if the grid frequency deviates by more than 10 mHz from its nominal 50 Hz. The maximum FCR response would be fully activated for a deviation of more than 200 mHz. The following

TABLE 2 Overview of the model parameters for dynamic simulations.

|			
Conduit length	L	60	m
Conduit diameter (RPT section, inlet)	$D_{1,2}$	6, 10	m
Pressure wave velocity	a	1000	m/s
Darcy friction factor	f	0.0158	—
Unsteady loss coefficient	k	0.04	m/s^2
Rotational inertia drivetrain 1	J_1	167 x 10^3	kg m^2
Rotational inertia drivetrain 2	J_1	237 x 10^3	kg m^2
Damping torque coefficient 1	$D_{f1,2}$	4137	Nm/rad/s
Damping torque coefficient 2	$D_{f1,2}$	6125	Nm/rad/s
Valve time constant	T_v	1.0	s
Minor loss coefficients			
Entrance	k_{en}	0.05	—
Exit	k_{ex}	1.0	—
Expansion	k_{exp}	0.04	—
Contraction	k_{con}	0.13	—

simulations assume the worst case scenario and aim to provide the full FCR provision as quickly as possible.

Since the proposed system operates over a wide range of operating conditions, the dynamic response is expected to differ, depending on the initial state. For instance, when the plant operates in turbine mode with an empty lower reservoir (indicating maximum energy capacity), the available head of the RPT reaches its peak value. Consequently, for a specific power change, the necessary change in flow rate is smaller compared to scenarios where the reservoir is nearly full and the head of the RPT is lower. To assess if the plant is capable of delivering the same amount of FCR independent of its state of charge, two cases in turbine mode are compared. In the first case, the RPT has an assumed gross head of 9 m stepping from 8 to 10 MW

per RPT unit (0.8 to 1 GW for the full plant). In the second case, the RPT has a gross head of 5 m available and steps from 2 to 4 MW per RPT unit. Figure 11 shows the simulated change of power setpoint for the first case.

When providing FCR in the Netherlands, the new power setpoint needs to be reached within 30 s [37]. This is defined as the power change period and the desired setpoint can be exceeded by up to 30%. The tolerances around the power setpoints are split into two sections. The allowed range in which 95% of the values must fall and the tolerable range in which a maximum of 5% may lie. The absolute tolerance is calculated based on the power setpoint and the percentage multiplied by the FCR power provided. After the power change period, a transient period of 90 s starts where the allowed range gives a 20% tolerance above and below the power setpoint and a tolerable range of 30%. Finally, after the transient period, the tolerances drop to 10 and 20%, respectively [38].

As can be observed from Figure 11, the system is able to reach its new power setpoint within around 3.5 s, thus easily fulfilling the requirements. To increase the power, the system needs to accelerate both runners resulting in a higher flow rate at the given head. To do so in a quick manner, the machine torques need to be reduced which explains the initial step-down in power. In order to fulfil the regulations while minimising the power change period, the initial torque step and minimum power are limited. In the presented simulation the initial step-down in power is limited to 20% of the provided reserve. If this step, while within the regulations, would be deemed undesirable, limiting the initial power reduction to 5% of the reserve, would only increase the power change period by about 1 s. The two machine torques and rotational speeds for this case are shown in Figure 12. Here this initial step-down in torque can be observed after which the torque is dropped further as the runners accelerate to maintain the minimum power setpoint. Once the rotational speeds approach their new desired setpoint
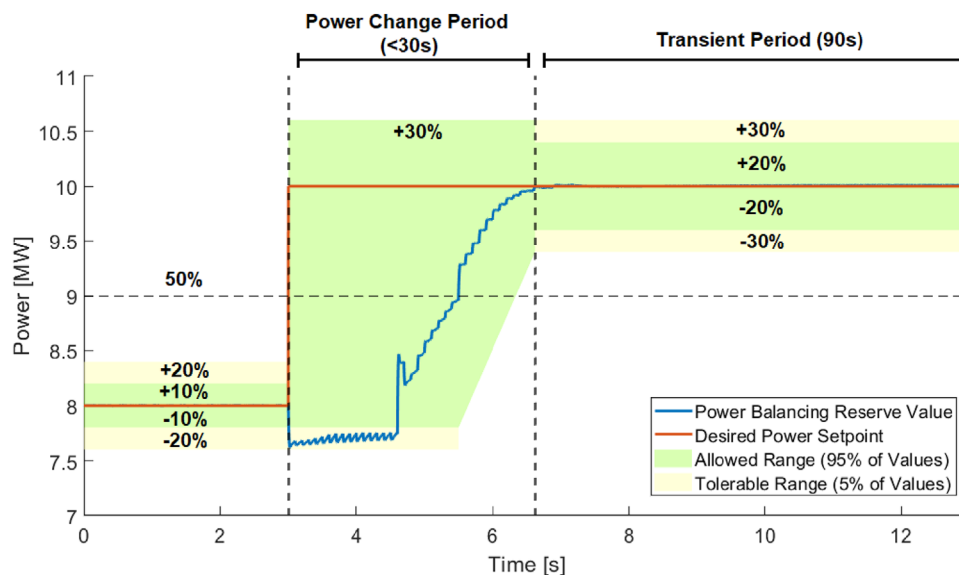
FIGURE 11 Power per RPT unit during a FCR simulation stepping from 8 to 10 MW.
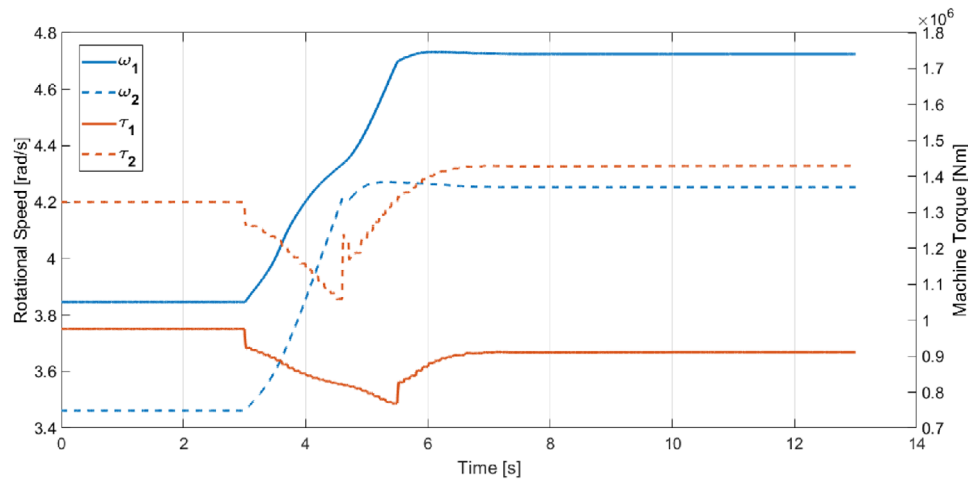
FIGURE 12   Rotational speeds and machine torques per RPT unit during a FCR simulation stepping from 8 to 10 MW.
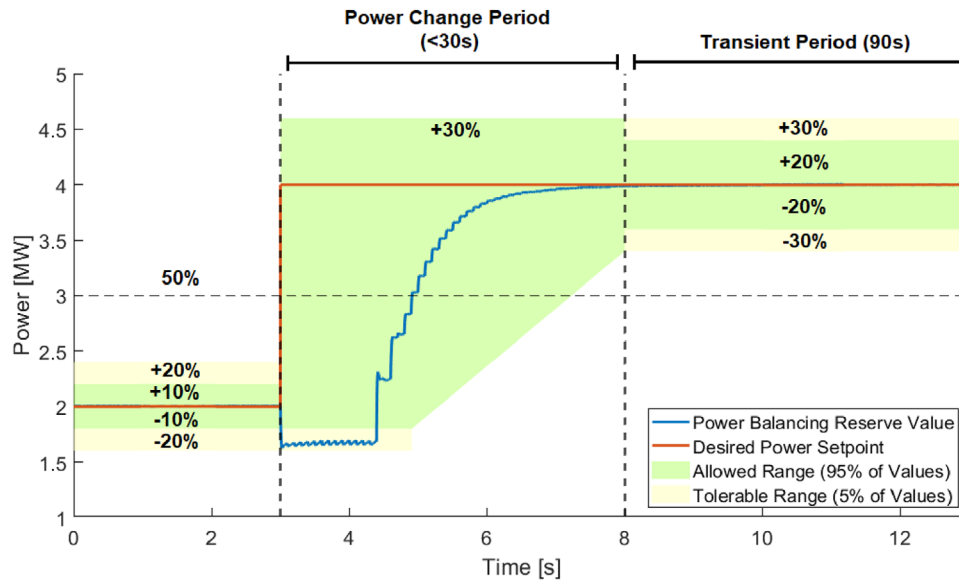
FIGURE 13   Power per RPT unit during a FCR simulation stepping from 2 to 4 MW.

the machine torques are increased to reduce the acceleration. The small fluctuations observed both in power and torque are caused by the speed control loop updating the current setpoint in 100 ms intervals.

Figure 13 shows the change of power for the second case. Most notably, the power change period here takes around 5 s and with that 40% longer than the previous case. This is explained through the larger change in flow rate of 22.6 m^3/s compared to a change of 15.4 m^3/s in the first case. The angular velocities of the runners also increase by around 1.05 rad/s compared to roughly 0.85 rad/s.

It is clear that this plant is capable to provide Frequency FCR across its entire operating range. With that, it is also equipped to offer other essential frequency regulation services, including automatic and manual frequency restoration reserves (aFRR &

mFRR). Notably, these services demand a less rapid adjustment of operating points compared to FCR. Additional components that may constrain the dynamic response of the system and are not covered in these results are the power electronics and grid side control. Their effect should be limited though compared to the physical inertias of the plant.

Among energy storage technologies, flywheels, supercapacitors and batteries are typically considered to have fast enough power ramp rates to provide frequency regulation services [39]. However, only battery storage offers large enough energy capacities to also provide balancing. With new technologies such as variable speed and hydraulic short circuit, existing conventional pumped storage plants have also been enabled to provide frequency regulation [40]. With a continuous reduction of spinning reserves in our power grids, providing ancillary services such

as FCR, aFRR and mFRR is a crucial component of energy storage systems to contribute to grid stability. Accordingly, providing these services opens up another revenue stream for the operator.

5 | CONCLUSION

This study has evaluated the potential and technical viability of a novel low-head pumped hydro storage system designed for coastal environments and shallow seas, focusing on its performance during energy balancing and capability to provide frequency regulation services. Both, a steady-state and dynamic modelling approach are used, centred on a case study applied to a prospective storage site in the Dutch North Sea. The findings from the conducted simulations have shown the potential to deploy the proposed low-head pumped storage technology at grid scale for both energy balancing and the provision of frequency regulation services. The system applied to the prospective site in the Dutch North Sea, has achieved round-trip efficiencies of over 70%. It was shown that using individual units of PMSMs at the nominal rating of 10 MW, severely constrain the wider operating range of the RPTs. By scaling up the electric machines alone, the full head range except for 1 m of the selected storage site can be utilised. This results in the reduction of the size of the reservoir required to reach the desired energy capacity of 4 GWh to approximately one third. Aside from this reduction in footprint, the average power during operation is also almost doubled.

The dynamic simulations that have been carried out show that fast power ramp rates across its operating range can be achieved. Allocating 20% of its nominal power for FCR, the new power setpoints are reached between 3.5 and 5 s for a full FCR response, depending on the initial state of charge. This fulfils FCR requirements with some margin, enabling it to participate in the provision of frequency regulation services. Based on this technical analysis, further studies investigating the economic and environmental viability of such a case should be carried out. Since both, balancing and frequency regulation services can contribute to the revenue for the operator, further optimisation of the energy management strategy can also help to improve the economic case and justify the high initial capital cost that is required for such a plant.

AUTHOR CONTRIBUTIONS

Justus Peter Hoffstaedt: Conceptualization; data curation; formal analysis; investigation; methodology; software; visualization; writing—original draft; writing—review and editing. **Daan Truijen**: Data curation; formal analysis; software; visualization; writing—original draft; writing—review and editing. **Antonio Jarquin Laguna**: Conceptualization; formal analysis; investigation; methodology; supervision; writing—original draft; writing—review and editing. **Jeroen De Kooning**: Supervision; writing—review and editing. **Kurt Stockman**: Supervision. **Jonathan Fahlbeck**: Resources; writing—review and editing. **Hakan Nilsson**: Resources; supervision; writing—review and editing.

CONFLICT OF INTEREST STATEMENT
The authors declare no conflict of interest.

DATA AVAILABILITY STATEMENT
The data that support the findings of this study are available from the corresponding author upon reasonable request.

ORCID
Justus Peter Hoffstaedt https://orcid.org/0000-0003-3320-8994
Antonio Jarquin Laguna https://orcid.org/0000-0002-9190-3373
Jeroen De Kooning https://orcid.org/0000-0002-0358-4350

REFERENCES
1. Al-Shetwi, A.Q., Hannan, M., Jern, K.P., Mansur, M., Mahlia, T.: Grid-connected renewable energy sources: Review of the recent integration requirements and control methods. J. Cleaner Prod. 253, 119831 (2020). https://www.sciencedirect.com/science/article/pii/S0959652619347018
2. Castillo, A., Gayme, D.F.: Grid-scale energy storage applications in renewable energy integration: A survey. Energy Convers. Manage. 87, 885–894 (2014). https://www.sciencedirect.com/science/article/pii/S0196890414007018
3. Qudaih, M., Engel, B., Truijen, D.P.K., De Kooning, J.D.M., Stockman, K., Hoffstaedt, J.P., Jarquin-Laguna, A., Ruiz, R.A., Goseberg, N., de Vilder, L., Bricker, J.D., Joseph, M., Zangeneh, M., Terheiden, K.: The contribution of low-head pumped hydro storage to grid stability in future power systems. IET Renewable Power Gener. 17(14), 3594–3608 (2022). https://onlinelibrary-wiley-com.tudelft.idm.oclc.org/doi/full/10.1049/rpg2.12668
4. Johnson, D.O., Hassan, K.A.: Issues of power quality in electrical systems. Int. J. Energy Power Eng. 5, 148–154 (2016)
5. IEA. (2023) Tracking clean energy progress 2023. Online Report. https://www.iea.org/reports/tracking-clean-energy-progress-2023. Accessed 15 Nov 2023
6. Rehman, S., Al-Hadhrami, L.M., Alam, M.M.: Pumped hydro energy storage system: A technological review. Renew. Sustainable Energy Rev. 44, 586–598 (2015). https://www.sciencedirect.com/science/article/pii/S1364032115000106
7. Hoffstaedt, J.P., Truijen, D.P.K., Fahlbeck, J., Gans, L.H.A., Qudaih, M., Laguna, A.J., De Kooning, J.D.M., Stockman, K., Nilsson, H., Storli, P.-T., Engel, B., Marence, M., Bricker, J.D.: Low-head pumped hydro storage: A review of applicable technologies for design, grid integration, control and modelling. Renew. Sustainable Energy Rev. 158, 112119 (2022). https://www.sciencedirect.com/science/article/pii/S1364032122000478
8. Mongird, K., Fotedar, V., Viswanathan, V., Koritarov, V., Balducci, P., Hadjerioua, B., Alam, J.: Energy storage technology and cost characterization report. Tech. Rep., Pacific Northwest National Lab. (PNNL), Richland, WA (2019)
9. Pollitt, M.G., Anaya, K.L.: Competition in markets for ancillary services? the implications of rising distributed generation. Tech. Rep., Energy Policy Research Group, University of Cambridge (2019). http://www.jstor.org/stable/resrep30304

10. Prasasti, E., Aouad, M., Joseph, M., Zangeneh, M., Terheiden, K.: Optimization of pumped hydro energy storage design and operation for offshore low-head application and grid stabilization. Renew. Sustainable Energy Rev. 191, 114122 (2024). https://www.sciencedirect.com/science/article/pii/S1364032123009802

11. Ruiz, R.A., de Vilder, L., Prasasti, E., Aouad, M., De Luca, A., Geisseler, B., Terheiden, K., Scanu, S., Miccoli, A., Roeber, V., Marence, M., Moll, R., Bricker, J, Goseberg, N.: Low-head pumped hydro storage: A review on civil structure designs, legal and environmental aspects to make its realization feasible in seawater. Renew. Sustainable Energy Rev. 160, 112281 (2022). https://www.sciencedirect.com/science/article/pii/S1364032122002003

12. Prasasti, E., Joseph, M., Miao, X., Zangeneh, M., Terheiden, K.: Design of shaft- and rim-driven contra-rotating reversible pump-turbine to optimize novel low-head pumped hydro energy storages. Energy 306, 132237 (2024). https://www.sciencedirect.com/science/article/pii/S0360544224020115

13. Fahlbeck, J., Nilsson, H., Salehi, S., Zangeneh, M., Joseph, M.: Numerical analysis of an initial design of a counter-rotating pump-turbine. IOP Conf. Ser.: Earth Environ. Sci 774(1), 012066 (2021). https://doi.org/10.1088/1755-1315/774/1/012066

14. Shen, J., Pei, J., Wang, W., Yuan, S.: Instability characteristics regarding the saddle-shaped region in a reversible mixed-flow pump applied to the low-head pumped storage. J. Storage Mater. 63, 107035 (2023). https://www.sciencedirect.com/science/article/pii/S2352152X23004322

15. The Government of the Netherlands - Ministry of Economic Affairs and Climate Policy.: Climate agreement. https://www.government.nl/topics/renewable-energy/documents/reports/2019/06/28/climate-agreement. Accessed 6 Mar 2024

16. The Government of the Netherlands: Renewable energy - Offshore wind energy. https://www.government.nl/topics/renewable-energy/offshore-wind-energy. Accessed 6 Mar 2024

17. McIlwaine, N., Foley, A.M., Morrow, D.J., Kez, D.A., Zhang, C., Lu, X., Best, R.J.: A state-of-the-art techno-economic review of distributed and embedded energy storage for energy systems. Energy 229, 120461 (2021). https://www.sciencedirect.com/science/article/pii/S0360544221007106

18. VanGraafeiland, K.: Global tidal range. https://www.arcgis.com/home/item.html?id=d5354dea41b14f0689860bf4b2cf5e8a. Accessed 7 June 2023

19. Fahlbeck, J., Nilsson, H., Salehi, S., Zangeneh, M., Joseph, M.: Numerical analysis of an initial design of a counter-rotating pump-turbine. IOP Conf. Ser.: Earth Environ. Sci 774(1), 12066 (2021)

20. Truijen, D.P.K., Hoffstaedt, J.P., Fahlbeck, J., Laguna, A.J., Nilsson, H., Stockman, K., de Kooning, J.D.M.: Impact of dual variable speed and inlet valve control on the efficiency and operating range of low-head contra-rotating pump-turbines. IEEE Access 12, 86 854–86 868 (2024)

21. Brown, G.O.: The history of the Darcy-Weisbach equation for pipe flow resistance. In: Proceedings of the Environmental and Water Resources History, pp. 34–43. American Society of Civil Engineers, New York (2002). https://ascelibrary-org.tudelft.idm.oclc.org/doi/10.1061/40650%282003%294

22. Herschy, R.W., Rumney, G.R., Oliver, J.E., Mosley, M.P., Holland, P.G., Marsh, T.J., Collier, C.G., Yoshino, M.M., Herschy, R.W., Critchfield, H.J., Gilman, D.L., Collier, C.G., Holland, P.G.: Colebrook–White Equation. In: Encyclopedia of Hydrology and Water Resources, pp. 145–145. Springer, Dordrecht (1998). https://doi.org/10.1007/978-1-4020-4497-7_44

23. Stark, B., Andó, E., Hartley, G.: Modelling and performance of a small siphonic hydropower system. Renew. Energy 36(9), 2451–2464 (2011). https://www.sciencedirect.com/science/article/pii/S0960148111000887

24. Lubis, Z., Manik, T., Rinkanto, M., Sitorus, T.: Design of a heat exchanger of three concentric tube layer on contrary flow. IOP Conf. Ser.: Mater. Sci. Eng. 505, 012091 (2019)

25. Hoffstaedt, J.P., Jarquín-Laguna, A., Fahlbeck, J., Nilsson, H.: System model development and numerical simulation of low-head pumped hydro storage. In: Trends in Renewable Energies Offshore, pp. 757–763. CRC Press, Boca Raton (2022)

26. Wylie, E., Streeter, V.: Fluid transients in systems. J. Fluid Mech. 264, 375 (1994)

27. Stecki, J.S., Davis, D.C.: Fluid transmission lines-distributed parameter models Part 1: a review of the state of the art. Proc. Inst. Mech. Engrs. Part a 200(A4), 215–228 (1986)

28. Ghidaoui, M.S., Zhao, M., McInnis, D.A., Axworthy, D.H.: A review of water hammer theory and practice. Appl. Mech. Rev. 58(1), 49–76 (2005)

29. Chaudhry, M.H.: Applied Hydraulic Transients. Springer, New York (2014)

30. De Kooning, J.D.M., Vandoorn, T.L., Van de Vyver, J., Meersman, B., Vandevelde, L.: Displacement of the maximum power point caused by losses in wind turbine systems. Renew. Energy 85, 273–280 (2016). https://www.sciencedirect.com/science/article/pii/S0960148115300768

31. Hahn, H., Hau, D., Dick, C., Puchta, M.: Techno-economic assessment of a subsea energy storage technology for power balancing services. Energy 133, 121–127 (2017). https://www.sciencedirect.com/science/article/pii/S0360544217308733

32. Berrada, A., Emrani, A., Ameur, A.: Life-cycle assessment of gravity energy storage systems for large-scale application. J. Storage Mater. 40, 102825 (2021). https://www.sciencedirect.com/science/article/pii/S2352152X2100551X

33. Menéndez, J., Fernández-Oro, J.M., Galdo, M., Loredo, J.: Efficiency analysis of underground pumped storage hydropower plants. J. Storage Mater. 28, 101234 (2020). https://www.sciencedirect.com/science/article/pii/S2352152X20300323

34. Koohi-Fayegh, S., Rosen, M.: A review of energy storage types, applications and recent developments. J. Storage Mater. 27, 101047 (2020). https://www.sciencedirect.com/science/article/pii/S2352152X19306012

35. Chen, Y., Kang, Y., Zhao, Y., Wang, L., Liu, J., Li, Y., Liang, Z., He, X., Li, X., Tavajohi, N., Li, B.: A review of lithium-ion battery safety concerns: The issues, strategies, and testing standards. J. Energy Chem. 59, 83–99 (2021). https://www.sciencedirect.com/science/article/pii/S2095495620307075

36. Costa, C., Barbosa, J., GonÇalves, R., Castro, H., Campo, F.D., Lanceros-Méndez, S.: Recycling and environmental issues of lithium-ion batteries: Advances, challenges and opportunities. Energy Storage Mater. 37, 433–465 (2021). https://www.sciencedirect.com/science/article/pii/S2405829721000829

37. Tennet SOP-SYS: FCR Manual for BSP's. Tech. Rep., Tennet (2022). https://tennet-drupal.s3.eu-central-1.amazonaws.com/default/2023-04/Handboek%20FCR%20voor%20BSPs%20-%20EN%20version.pdf

38. 50hertz, Amprion, Tennet, Transnet BW.: Prequalification Process for Balancing Service Providers (FCR, aFRR, mFRR) in Germany ("PQ conditions"). Tech. Rep. (2022). https://www.regelleistung.net/Portals/1/downloads/regelenergieanbieter_werden/pr%C3%A4qualifikationsbedingungen/PQ%20Bedingungen%20-%2003.06.2022%20(englisch).pdf?ver=4rD5rRjAmi_tqY0oI3Q2Mw%3d%3d

39. Akram, U., Nadarajah, M., Shah, R., Milano, F.: A review on rapid responsive energy storage technologies for frequency regulation in modern power systems. Renewable Sustainable Energy Rev. 120, 109626 (2020). https://www.sciencedirect.com/science/article/pii/S1364032119308330

40. Ma, X., Wu, D., Wang, D., Huang, B., Desomber, K., Fu, T., Weimar, M.: Optimizing pumped storage hydropower for multiple grid services. J. Storage Mater. 51, 104440 (2022). https://www.sciencedirect.com/science/article/pii/S2352152X22004637